

Article

Not peer-reviewed version

---

# Cellular Compartmentalization as a Physical Regulation of Biological Processes

---

[Ahmed Naser Fayad](#) , Diego Mazo-Durán , [David G. Miguez](#) \*

Posted Date: 9 October 2024

doi: 10.20944/preprints202410.0593.v1

Keywords: signaling pathway; mathematica modeling



Preprints.org is a free multidiscipline platform providing preprint service that is dedicated to making early versions of research outputs permanently available and citable. Preprints posted at Preprints.org appear in Web of Science, Crossref, Google Scholar, Scilit, Europe PMC.

Copyright: This is an open access article distributed under the Creative Commons Attribution License which permits unrestricted use, distribution, and reproduction in any medium, provided the original work is properly cited.

## Article

# Cellular Compartmentalization as a Physical Regulation of Biological Processes

Ahmed N. Fayad <sup>1,2,3,†</sup>, Diego Mazo-Durán <sup>1,2,3,†</sup> and David G. Míguez <sup>1,2,3,\*</sup>

<sup>1</sup> Centro de Biología Molecular Severo Ochoa, Universidad Autónoma de Madrid, 28049 Madrid, Spain

<sup>2</sup> Instituto de Física de la Materia Condensada, Facultad de Ciencias, Universidad Autónoma de Madrid, 28049 Madrid, Spain

<sup>3</sup> Instituto de Física de la Materia Condensada, Uni

\* Correspondence: david.miguez@uam.es

† ANF contributed equally to this work with DP.

**Abstract:** Cells compartmentalize biochemical processes taking advantage of physical barriers in the form of membranes. Eukaryotes have a wide diversity of membrane-based compartments that can be used in this context, with the main ones being the extracellular membrane, which separates the inside from the outside of the cell, and the nuclear membrane, that separates the nucleus from the cytoplasm. The nuclear membrane not only isolates and protects the DNA and the transcription and replication processes from the other processes that are taking place in the cytoplasm, but also has an active role in the regulation of cellular signaling. The TGF- $\beta$  pathway is one of the most important and conserved signaling cascades, and it takes advantage of compartmentalization using a well-tuned balance between import and export rates of active and inactive forms of key proteins. Thus, compartmentalization serves as an additional regulatory mechanism, physically isolating transcription factors from their targets, influencing the dynamics and strength of signal transduction. This contribution focuses on this biophysical layer of regulation. It begins with an in-depth review of the TGF- $\beta$  pathway and the main regulatory processes underlying this compartmentalization mechanism. Next, we focus on several contributions that study how this compartmentalization shapes the dynamics and ultimately the cell response, and how this separation can be used as readout of several cellular responses. Finally, we introduce a simplified mathematical approach to study this process derived using a generalized formulation.

**Keywords:** biophysical; TGF- $\beta$ ; Smad; translocation; systems; modeling

The development and organization of multicellular organisms are mainly regulated by intercellular communication in the form of signaling molecules [1]. These molecules trigger intracellular events that are processed by the cell in the form of signaling pathways that ultimately lead to changes in the expression, regulation, and dynamics of proteins. Most of these regulatory events are biochemical in nature, e.g., reversible covalent addition of a phosphate group (phosphorylation), sugar molecules (glycosylation), ubiquitin proteins (ubiquitination), acetyl groups (acetylation), and methyl groups (methylation). These posttranslational modifications can alter many aspects of the target proteins: phosphorylation can activate or deactivate enzymes and signaling proteins, acetylation of histones can alter DNA-protein interactions, glycosylation can affect protein folding and stability, methylation can affect the dynamics of protein-protein interactions, and ubiquitination can target a protein for degradation [2].

In addition to these biochemical mechanisms, there are other type of regulatory mechanism that involve physical constraints. One of the most studied is protein compartmentalization, i.e., intracellular proteins can be directed to specific organelles or regions within the cell, such as the nucleus or the cell membrane. In addition to providing and maintaining organization at the cellular level, this physical separation of processes is highly dynamic (proteins can change location due to specific signals) and has a strong biological regulatory impact [3]. For instance, constraining a given enzyme to a specific region results in a localized increase in concentration, enhancing its efficiency. One of the most important cases is the compartmentalization of glucokinase, which can shift location in response to substrate availability [4]. In brief, a fraction of the glucokinase can translocate from the nucleus to the cytoplasm after stimulation, resulting in reduction in its nuclear to cytoplasmic ratio. Another important protein subjected to compartmentalization is Rubisco, a crucial enzyme in photosynthesis and carbon fixation.

This compartmentalization has been shown to affect its catalytic efficiency and, in consequence, the overall photosynthetic rate in plants [5]. Interestingly, Compartmentalization is suggested to restrict the conformational variability of the protein, shaping the evolution of all living organisms that harvest energy via photosynthesis [6].

In our lab, we have focused on this concept of compartmentalization in the context of dimensionality reduction [7–10]. This concept refers to the transition from moving in a three-dimensional space (the cytoplasm) to a two dimensional space when molecules are embedded or associated with the cell membrane [10]. This shift from 3D to 2D movement results in a important change in local concentration, increasing by orders of magnitude the probability of molecular encounters and interactions, and in consequence, the rate of biochemical reactions [9].

This way, the association of a protein or ligand to a receptor in the membrane catalyzes subsequent reactions by restricting the movement of the ligand to the membrane surface, resulting in an effective increase in its local concentration because the volume in which the molecules can move is significantly reduced; this mechanism of action drives the dynamics of activation of erythropoietin (EPO) [10], and it is the basis of our design of drugs that can selectively affect tumor cells versus normal cells [7–9].

The bidirectional movement of transcription factors between the nucleus and cytoplasm in eukaryotic cells is a common example of intracellular compartmentalization. This exchange of proteins that are dynamically excluded from the cytoplasm or the nucleus is essential for various cellular functions, including gene expression, signal transduction, and cell cycle regulation. Dysregulation of nuclear translocation has been shown to be directly involved in a variety of pathological conditions, with a critical role in maintaining cellular homeostasis.

One of the most important pathways that take advantage of this nucleocytoplasmic shuttling to modulate signal transduction is the transforming growth factor  $\beta$  (TGF- $\beta$ ), involved in the regulation of a wide range of signaling functions, from tissue-specific control of development, morphogenesis, cell proliferation and differentiation, tissue homeostasis, regeneration, and even cell-specific or tissue-specific motility [11]. It also has been shown to have a growth-inhibitory effect on epithelial cells, suggesting a tumor suppressor role in carcinomas and cell fate determination [12].

In this review, we focus on the effect of transcription factor compartmentalization in the context of the TGF- $\beta$ , and how this physical regulation is utilized to modulate signal transduction. We start with a review of the main aspects of the pathway, followed by several key studies that investigated how this nucleocytoplasmic translocation shapes the dynamics of the signal. We finalize with an illustration of how mathematical modeling can be applied in the context of protein compartmentalization to study these type of biophysical aspects of biological regulation.

### The TGF- $\beta$ Pathway Signaling Dynamics and Regulation

The TGF- $\beta$  signaling pathway takes its name from the main extracellular signal that activates the cascade of downstream events: the human transforming growth factor  $\beta$  (TGF- $\beta$ ) ligand superfamily. These dimeric polypeptide growth factors involves thirty-three secreted cytokines [13,14], and the different family members have been given various names according to their molecular identification history: TGF- $\beta$ s (three isoforms of TGF- $\beta$ s: TGF- $\beta$ 1, TGF- $\beta$ 2 and TGF- $\beta$ 3), Activins, Bone Morphogenetic Proteins (BMPs), Growth Differentiation Factors (GDFs), Nodal and Müllerian Inhibiting Substance (MIS) [15]. Interestingly, this superfamily of signaling molecules is one of the most conserved throughout the animal kingdom, and it is believed to have originated in the early stages of multicellular evolution [16].

Canonical TGF- $\beta$  signaling starts by the reversible binding of one of these dimeric ligands to two transmembrane receptors (TGF $\beta$ RII). After binding, these receptor molecules undergo a conformational change that facilitates their interaction with two other transmembrane receptors (TGF $\beta$ RI) [1]. The result is the formation of a heterotetrameric complex composed of two TGF $\beta$ RII and two TGF $\beta$ RI molecules, represented as (TGF $\beta$ RII)-(TGF $\beta$ RI) [17]. Once the receptor complex is formed [18], the type-II receptors phosphorylate and activate the type-I kinase receptor, following endocytosis inside

vesicles characterized by the presence of the Smad Anchor for Receptor Activation protein (SARA) on their membrane. Once inside the endosomes, the type-I receptors phosphorylate and activate downstream proteins (Figure 1).

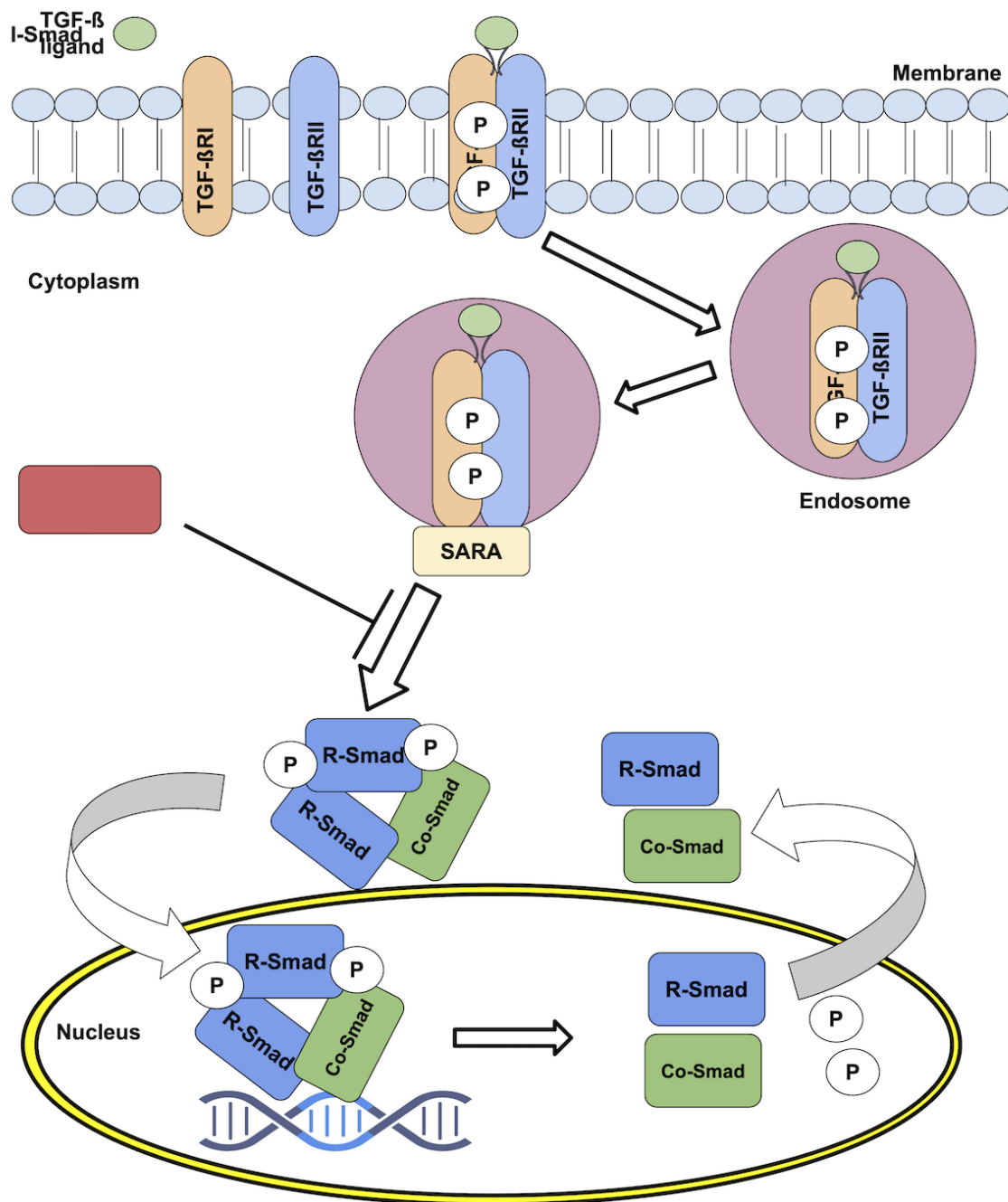


**Figure 1.** Signaling through TGF- $\beta$  superfamily ligands (adapted from Ref. [19]. Explain .

These Smad proteins, which give name to the endosomes, are themselves the main effectors of the signaling events mediated by TGF- $\beta$  ligand stimulation. The Smads are a family of transcription factors (i.e., they bind directly to DNA) highly conserved throughout evolution, and come in three flavours: The first type is R-Smad (receptor-regulated Smads), which includes Smad1, 2, 3, 5, and 8. [16]. The second type is Co-Smad (common mediator Smads) or Smad4, which serves as cofactor of the R-Smads [20,21]. The third type is I-Smads (inhibitory Smads), including Smad6 and 7, that inhibit R-Smads activation by interfering with their phosphorylation by the receptor complexes [20,22].



### R-Smads Nucleocytoplasmatic Shuttling as a Modulation of Signal Transduction

As mentioned before, the R-Smads constitute the direct substrates of TGF- $\beta$  family receptors and the key mediators of the TGF- $\beta$  pathway. They serve as key mediators of the TGF- $\beta$  pathway, translating receptor activation into changes in gene expression levels. All R-Smads share a common molecular structure, consisting of two conserved globular domains: N-terminal MH1 (Mad Homology 1), responsible mainly for direct DNA binding, and C-terminal MH2 (Mad Homology 2) domain, responsible mainly for receptor interaction. Both domains are connected by a linker region that is not conserved, but contains multiple phosphorylation sites for various kinases that regulate the function and activation of the different R-Smads. Two main sets of R-Smads can be identified depending on their specific receptor: Smad2 and Smad3 are activated via TGF- $\beta$  and Activin/Nodal [23], while the rest are mainly activated by BMP receptors [16,19,24–26].

One of the main characteristics of R-Smads is their ability to translocate from the cytoplasm to the nucleus, depending on their phosphorylation state and organization as monomers or complexes. The sequence of events in this well characterized process, commonly refereed as Smad nucleocytoplasmic shuttling, occurs as follows: (a) Unphosphorylated R-Smads are mainly located in the cytoplasm as monomers;; (b) after activation by the type-I receptor, two R-Smads typically assemble with one Co-Smad in the form of heterotrimers, also known as the activated Smad complex (the complex is stabilized by the phosphorylated serines at the C-terminal); (c) these complexes then translocate into the nucleus where they act as transcription factors [27,28]; (d) These complexes are then dephosphorylated via interaction with PPM1A and other phosphatases [29], and this dephosphorylation has been linked to destabilization of the trimer complex [30]; (e) Once dephosphorylated, the complexes disassemble, (f) finally, the monomeric R-Smads and Smad4 are exported separately back to the cytoplasm by distinct mechanisms [30].

The two main processes involved in this shuttling are nuclear import and nuclear export through the nuclear pore complex (NPC), a large protein structure embedded in the nuclear envelope that serves as a gateway for selective transport of molecules between the nucleus and cytoplasm. In brief, the NPCs act as hydrophobic channels [31] that [32] allow proteins smaller than 20–30 kDa to pass by diffusion, While larger proteins require active transport mediated by importin and exportin receptors [33–35].

### Dynamics and Regulation of Export and Import of the R-Smads

Over the past years, several studies have used this different levels of R-Smad protein in the nucleus or cytoplasm to study the mechanisms that regulate this process [29]. These studies have shown that the import activity of the R-Smad complexes rely on the interaction of importins with the MH1 domain (specifically importin- $\beta$ 1 [36], but also importin 7 and 8 [37], in a process that depends on the RanGTP/GDP gradient across the nuclear membrane. On the other hand, it has been proposed that Smad2 can also enter the nuclei via direct interaction of proteins of the NPCs with its MH2 domain [30]. Additionally, several experimental studies propose that not only multimeric Smads (i.e., as part of complexes) can enter the nuclei, but also monomeric Smads can be imported into the nucleus through a mechanism different than the R-Smad complexes [30].

Regarding nuclear export, it has been proposed that R-Smads monomers exit the nucleus mediated by exportin 4 [16,38,39], but not exporting 1 (the target of Leptomycin B [40]). The export mechanism of the R-Smads has been shown to depend on a Ran-GTPase and Ran-BP3, which recognizes unphosphorylated R-Smad protein resulting from the activity of nuclear R-Smad phosphatases, such as PPM1A [41]. Similarly to the import process, Smad2 has been proposed to be able to also exit the nucleus by direct interaction with the proteins of the NPCs [42,43]. This is consistent with the lack of the Lys-rich KKLKK sequence in its MH1 domain that is critical for nuclear export of Smad3 [44].

As a result of this complex regulation, R-Smads at the cytoplasm are mainly in the form of unphosphorylated monomers, while after activation, they primarily locate inside the nucleus, mostly in the form of complexes. The concentration of R-Smads monomers or complexes in each compartment

is determined by the differences in their import and export rates. This way, the higher concentration in the cytoplasm of R-Smads unphosphorylated monomers results from a slower import rate and a faster export rate, compared to the complexes [45]. Each of these rates depends on the ability of R-Smads to interact with NPCs, importins, and exportins in monomer or complex configuration [45,46].

On the other hand, the Smad4 monomer can be found in both the nucleus and the cytoplasm [47] due to similar rates of movement into and out of the nucleus, while when part of a complex, it is mainly located inside the nucleus, following the dynamics dictated by the other components of the complex (R-Smads) [48]. Interestingly, other studies show that inhibition of CRM1 or exportin 1 leads to rapid accumulation of Smad4 in the nucleus, suggesting that also Smad4 is actively translocating [40], therefore the mechanisms of Smad4 translocation and its impact in the translocation of the active complex needs further study.

### Taking Advantage of Nucleoplasmatic Shutting to Study the TGF- $\beta$ Pathway

An advantage of these differential R-Smad levels in cellular compartments is that they can be used as simplified readouts of changes in TGF- $\beta$  pathway activation, measurable by microscopy. These type of studies rely on direct visualization of the R-Smads or Co-Smads with fluorescence or photoactivatable fusion proteins [49], or the use of highly reliable and specific antibodies that can be used to measure changes in relative levels and compare this way experimental conditions in fixed sample. For instance, the seminal contribution by the lab of Caroline Hill [46] used FLAG tagged Smad4 and antibodies against Smad2 and Smad3 to show that inhibition of CRM1-mediated nuclear export results in very fast Smad4 nuclear accumulation, while endogenous Smad2 and Smad3 remained completely unaffected. Another contribution from the same lab [29,50], developed a fusion of Smad2 with GFP to follow *in vivo* the difference in translocation in unstimulated versus TGF- $\beta$ -stimulated cells. This study showed that the nuclear accumulation of the active form of Smad2 is due to a decrease in the rate of nuclear export of the protein, rather than an increase in import [29]. Moreover, it suggests that the import rate of phosphorylated R-Smads (in complex configuration) and unphosphorylated R-Smads (mainly in monomer configuration) is similar, indicating that import proteins act similarly in activated and deactivated states. If this is correct, the import rate of R-Smads as complexes should be twice as fast as the R-Smads as monomers, since each complex is composed of two molecules of R-Smad. On the other hand, the fact that the rate of export of the phosphorylated form of the R-Smads is much smaller than the rate of export when unphosphorylated suggests that maybe the configuration as complexes prevents the binding with exportin 4.

Another important example that utilizes the nucleocytoplasmic shuttling was performed by the Liu lab [51], where they study how variable dose levels of ligand are translated into intracellular signaling dynamics, and how continuous ligand doses can be translated into discontinuous cellular fate decisions. In this study, They show that the pathway processes continuous and pulsating TGF- $\beta$  ligand levels differently, displaying varied sensitivities to short and long pulses, also showing that it displays different sensitivities in response to short and long pulses of ligand. These two types of dynamic responses may be crucial for the role of the TGF- $\beta$  pathway in mediating stem cell differentiation.

The differential concentration of R-Smads as a readout is also used [52] to study the temporal signals by the TGF- $\beta$  pathway and its implications for embryonic patterning. This time, authors take advantage of the nuclear accumulation dynamics of a GFP-Smad4 fusion protein to measure TGF- $\beta$  pathway activity in response to different types of ligand stimulation. The same fusion protein was used to show pulsatile behaviors in Smad4 nuclear localization [48]. Similarly, quantitative measurements of Smad2/3 nuclear localization have illustrated that the TGF- $\beta$  pathway exhibits fold-change detection properties [53], i.e., cells respond to relative rather than absolute levels of TGF- $\beta$ . In other context, the accumulation of the R-Smads in the nucleus was the main readout to study the crosstalk between oncogenic Ras and TGF- $\beta$  signaling [54], since Ras activation inhibits the TGF- $\beta$ -induced nuclear accumulation of Smad2 and Smad3.

In our lab, we have studied how different R-Smad accumulations influence the role of the TGF- $\beta$  signaling cascade in vertebrate spinal cord formation [55,56]. In these studies, In this way, we quantified changes in the nuclear localization of the two R-Smads to explore the effects of the interplay between Smad2 and Smad3. We showed that the heterotrimers Smad2-Smad3-Smad4 induce cooperation and antagonism in the activation of the targets of the two R-Smads and that this dual role strongly influences the balance between neural stem cell proliferation and differentiation [55]. Using immunofluorescence and confocal imaging, we visualized and quantified R-Smad expression patterns at different developmental stages, showing pathway activation (i.e., R-Smads become more nuclear) in the transition zone (where stem cells cycle and perform interkinetic nuclear migration) and the differentiated zone (where differentiated neurons migrate after exiting the cell cycle). The study was complemented by numerical simulations, which allowed us to interpret the dual antagonism and cooperativity arising from heterotrimer assembly [55].

### Mathematical Modeling of Regulatory Compartmentalization

Mathematical modeling in molecular biology is a complementary approach to the more time consuming and expensive experimental approach, that can help explain results, make predictions and test hypotheses that will complement experimental studies. In the context of the TGF- $\beta$  signaling, several key contributions have combined modeling approaches with experimental results to try to understand different aspects of the regulation of compartmentalization as a physical regulation of gene expression [51,55,57].

One of the earliest approaches to studying the TGF- $\beta$  pathway dynamics using numerical simulations focused on the dynamics in experiments of fluorescent recovery after photobleaching (FRAP) [57]. Their results support the hypothesis that there is a dynamic maintenance of Smad nuclear accumulation during signaling [57]. In another study, the authors develop a model that shows how cells can integrate repeated pulses and maintain the phosphorylated Smad2 concentration [51]. Their main conclusion derived from the model is that the pathway is able to respond with different sensitivity to different ligand doses and time scales [51].

One main caveat of these early approaches is that the models used are composed of around 20 ordinary differential equations to make the predictions, making them very difficult to interpret. More recent examples have opted for more simplified mathematical formulations, for instance using the “pseudo-steady-state” approximation, or “rapid equilibrium assumption” to reduce the network signalling reactions based on an analysis of the different time scales of the individual reactions [58]. This model predicted a critical role of potential positive and delayed negative feedback loops on the regulation of the TGF- $\beta$  signalling system.

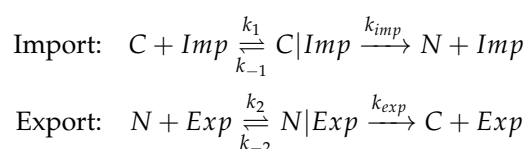
In line with simplified models, composed of the minimal set of equations required for explaining experimental observations, we developed a mathematical model based on differential equations to support the hypothesis that the heterotrimer Smad2-Smad3-Smad4 was being formed during vertebrate neurogenesis and that its formation could explain the fact that Smad2 and Smad3 antagonize in some targets, while cooperate in activating transcription of others [55]. The model prediction was then validated using immunoprecipitation [55].

In this section, we propose in the same philosophy of simple modeling approaches, a very simple yet powerful mathematical approach to study the dynamics of this nucleocytoplasmic shuttling. The model is designed with ordinary differential equations derived using the mass action law, and is used to reproduce the dynamics of a R-Smad protein in and out of the nuclei. From this simplified system, it is easy to study the main mechanisms and parameters that affect this dynamic equilibrium without needing to perform complicated calculations or simulations.

To build the model, let's consider a R-Smad protein inside of a cell, that can enter and exit the nucleus. These two potential states of the R-smad protein will be represented in the model as C (for cytoplasmic) and N (for nuclear). Based on the molecular details of the process reviewed above, we know that the processes crossing the NPCs are actively mediated by interaction with other

proteins, that we will call *Imp* (for import) and *Exp* (for export). This way, to enter into the nucleus, a cytoplasmic molecule *C* must be linked to the import enzyme *Imp*, and form a complex *C|Imp*. This complex, is then allowed to enter the nucleus. Once in the nucleus, the *C|Imp* complex gets disassembled into one molecule *N* (since now the R-Smad molecule is inside the nucleus) and the *Imp* enzyme.

Similarly, the export process follows the same rationale: the nuclear molecule *N* binds to export enzyme *Exp*, forming the *N|Exp* complex. This complex is now able to cross the NPCs and translocate to the cytoplasm. Once in the cytoplasm, the complex is disassembled, giving one *C* (our molecule is now in cytoplasmic configuration again) and the enzyme *Exp*. The rates of the nuclear import and export processes for *C|Imp*, and *N|Exp* complexes are  $k_{imp}$ ,  $k_{exp}$ , respectively. The formation rates of *C|Imp* and *N|Exp* are  $k_1$  and  $k_2$ , respectively. We will include in the model the fact that the complex formation is a reversible process, which means that the complex can spontaneously disassemble before crossing the NPCs. Dissociation rates of *C|Imp* and *N|Exp* are labeled as  $k_{-1}$  and  $k_{-2}$ , respectively. On the other hand, the dissociation of each complex once it crosses the NPCs is considered to be instantaneous, while *Imp* and *Exp* transport enzymes can translocate freely between the nucleus and cytoplasm (they are not limiting reagents) [59,60]. The whole system of interactions can be illustrated using a chemical reaction formalism as:



The scheme of the interaction is illustrated in Figure 2.

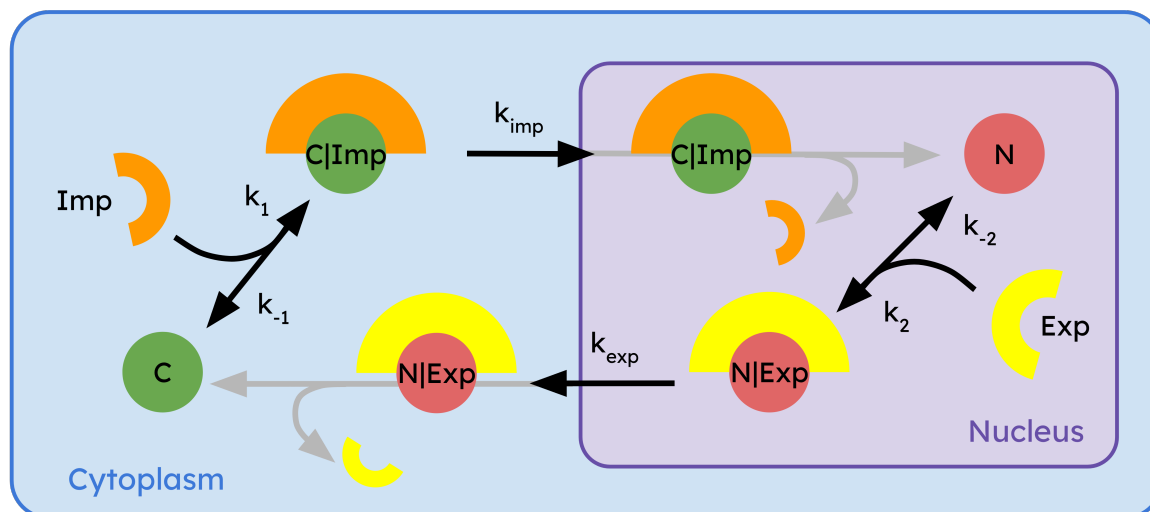


**Figure 2.** Schematic representation of the nuclear import-export process of a molecule inside a cell. The molecule in the cytoplasm is represented by *C*, and in the nucleus by *N*. To be imported inside the nucleus, the one *C* molecule must bind one molecule of the import enzyme *Imp*. Then, the complex *C|Imp* can enter the nucleus, where it disassembles into *N* (former *C*) and *Imp*. The export process is analogous, involving the formation of a *N|Exp* complex (one molecule of *N* and one export enzyme *Exp*) and then the disassembly of this complex in the cytoplasm yielding one molecule of *C* and one molecule of *Exp*.

#### Using the Mass Action Law to Model a Biological System

To translate this system of interactions into differential equations, we will use the the mass action law formalism, a fundamental principle in the mathematical modeling of chemical and biological



systems. In brief, the law of mass actions states that the rate of change of a species involved in a chemical interaction with other species is directly proportional to the product of the masses of the reactants, each raised to a power equal to the coefficient used in the chemical equation. Initially proposed for chemical systems by Cato Guldberg and Peter Waage in 1864 [61] based on previous work by Claude Louis Berthollet [62], and further clarified by Jacobus van 't Hoff in 1877 [63], it also provides a simplified yet effective framework for quantifying biological interactions.

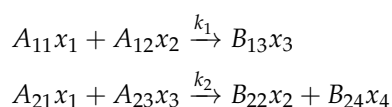
To illustrate the process of using the mass action to derive differential equations, let's consider first a general system in which several  $n$  species  $x_1, x_2, \dots, x_n$  interact with each other by means of a set of  $m$  chemical reactions, with rate constants  $k_1, k_2, \dots, k_m$ . The concentration of the species  $x_j$  is expressed as  $[x_j]$ . We start with the definition of a column vector that contains the concentrations of all species at a given time point. This vector is labeled as the *state vector*.

$$[\vec{X}] = \begin{pmatrix} [x_1] \\ [x_2] \\ \vdots \\ [x_n] \end{pmatrix}$$

Next, we define a square matrix of  $(m \times m)$  that contains all the rate constants in its diagonal. This matrix  $K$  is as follows:

$$K = \begin{pmatrix} k_1 & 0 & \cdots & 0 \\ 0 & k_2 & \ddots & \vdots \\ \vdots & \ddots & \ddots & 0 \\ 0 & \cdots & 0 & k_m \end{pmatrix}$$

Next, we define two  $m \times n$  matrices  $A$  and  $B$ , that contain the stoichiometric coefficients of reactants and products, respectively. In this matrices value of the  $A_{ij}$  element is the stoichiometric coefficient of the species  $j$  as reactant in reaction  $i$ , while the value of the  $B_{ij}$  element is the stoichiometric coefficient of the species  $j$  as a product in reaction  $i$  (in the sub indices notation,  $i$  and  $j$  denote rows and columns, respectively). If any of these coefficients does not appear in the reactions, then it is set to zero. For example, in the system:



the species concentration vector and the rate constants matrices are:

$$[\vec{X}] = \begin{pmatrix} [x_1] \\ [x_2] \\ [x_3] \\ [x_4] \end{pmatrix} \quad K = \begin{pmatrix} k_1 & 0 \\ 0 & k_2 \end{pmatrix}$$

and, since  $x_3$  and  $x_4$  do not appear as reactants in reaction 1, we set  $A_{13} = A_{14} = 0$ . In a similar manners, since  $x_2$  and  $x_4$  do not appear as reactants in reaction 2, we set  $A_{22} = A_{24} = 0$ . The same rationale is applied to construct matrix  $B$ , giving the following stoichiometric matrices:

$$A = \begin{pmatrix} A_{11} & A_{12} & 0 & 0 \\ A_{21} & 0 & A_{23} & 0 \end{pmatrix} \quad B = \begin{pmatrix} 0 & 0 & B_{13} & 0 \\ 0 & B_{22} & 0 & B_{24} \end{pmatrix}$$

Finally, we define a column vector  $[\vec{X}]^A$  of  $m$  rows, that contains in each row the product of all the species raised to the power of the corresponding  $A$  matrix coefficient. This way the  $i$ -th row of this vector can be calculated as:

$$([\vec{X}]^A)_i = \prod_{j=1}^n [x_j]^{(A_{ij})} \quad (1)$$

As an example, this vector for the previous reaction can be calculated as:

$$[\vec{X}]^A = \begin{pmatrix} [x_1]^{A_{11}} [x_2]^{A_{12}} [x_3]^0 [x_4]^0 \\ [x_1]^{A_{21}} [x_2]^0 [x_3]^{A_{23}} [x_4]^0 \end{pmatrix} = \begin{pmatrix} [x_1]^{A_{11}} [x_2]^{A_{12}} \\ [x_1]^{A_{21}} [x_3]^{A_{23}} \end{pmatrix}$$

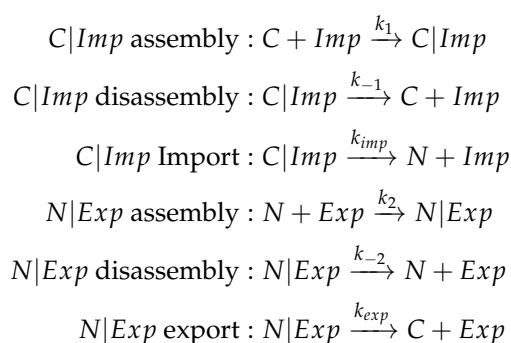
With all these definitions, the mass action law states that the temporal evolution of the concentration of the species is given by:

$$\frac{d[\vec{X}]}{dt} = (B - A)^t \cdot K \cdot [\vec{X}]^A \quad (2)$$

where the elements of the  $(B - A)^t$ , which is a  $n \times m$  matrix, are given by

$$[(B - A)^t]_{ij} = B_{ji} - A_{ji} \quad (3)$$

Now, let's apply the previous recipe to our system of nuclear translocation. To do that, we first need to separate each reaction as an individual process, in a way that each reversible interaction is equivalent to two irreversible interactions. This way, the system of interactions for import and export can be decompose as the following six coupled processes:



The next step is to apply the mass action law, to obtain six ordinary differential equations (ODEs, one for each species in the system) that will show the temporary evolution of the concentration of the species once solved. We have 6 reactions and 6 species, therefore we first define the state vector as:

$$[\vec{X}] = \begin{pmatrix} [C] \\ [Imp] \\ [C|Imp] \\ [N] \\ [Exp] \\ [N|Exp] \end{pmatrix}$$

containing the concentration of the species  $[\vec{X}]$  and a diagonal matrix  $K$  containing the rates of the reactions (in the order shown above):

$$K = \begin{pmatrix} k_1 & 0 & 0 & 0 & 0 & 0 \\ 0 & k_{-1} & 0 & 0 & 0 & 0 \\ 0 & 0 & k_2 & 0 & 0 & 0 \\ 0 & 0 & 0 & k_{-2} & 0 & 0 \\ 0 & 0 & 0 & 0 & k_{imp} & 0 \\ 0 & 0 & 0 & 0 & 0 & k_{exp} \end{pmatrix}$$

Considering the order of the reactions in  $K$  and the order of the species as they appear in  $[\vec{X}]$ , we can define matrices  $A$  and  $B$  as:

$$A = \begin{pmatrix} 1 & 1 & 0 & 0 & 0 & 0 \\ 0 & 0 & 1 & 0 & 0 & 0 \\ 0 & 0 & 0 & 1 & 1 & 0 \\ 0 & 0 & 0 & 0 & 0 & 1 \\ 0 & 0 & 1 & 0 & 0 & 0 \\ 0 & 0 & 0 & 0 & 0 & 1 \end{pmatrix}$$

$$B = \begin{pmatrix} 0 & 0 & 1 & 0 & 0 & 0 \\ 1 & 1 & 0 & 0 & 0 & 0 \\ 0 & 0 & 0 & 0 & 0 & 1 \\ 0 & 0 & 0 & 1 & 1 & 0 \\ 0 & 1 & 0 & 1 & 0 & 0 \\ 1 & 0 & 0 & 0 & 1 & 0 \end{pmatrix}$$

Now, we compute the  $[\vec{X}]^A$  vector for this systems as:

$$[\vec{X}]^A = \begin{pmatrix} [C][Imp] \\ [C|Imp] \\ [N][Exp] \\ [N|Exp] \\ [C|Imp] \\ [N|Exp] \end{pmatrix}$$

Next, we calculate the transpose matrix of  $(B - A)$ , which is denoted as  $(B - A)^t$ :

$$(B - A)^t = \begin{pmatrix} -1 & 1 & 0 & 0 & 0 & 1 \\ -1 & 1 & 0 & 0 & 1 & 0 \\ 1 & -1 & 0 & 0 & -1 & 0 \\ 0 & 0 & -1 & 1 & 1 & 0 \\ 0 & 0 & -1 & 1 & 0 & 1 \\ 0 & 0 & 1 & -1 & 0 & -1 \end{pmatrix}$$

Finally, to obtain the ODE system we use the mass action law in Equation 2, yielding to:

$$\begin{aligned}\frac{d[C]}{dt} &= -k_1[C][Imp] + k_{-1}[C|Imp] + k_{exp}[N|Exp] \\ \frac{d[Imp]}{dt} &= -k_1[C][Imp] + k_{-1}[C|Imp] + k_{imp}[C|Imp] \\ \frac{d[C|Imp]}{dt} &= k_1[C][Imp] - k_{-1}[C|Imp] - k_{imp}[C|Imp] \\ \frac{d[N]}{dt} &= -k_2[N][Exp] + k_{-2}[N|Exp] + k_{imp}[C|Imp] \\ \frac{d[Exp]}{dt} &= -k_2[N][Exp] + k_{-2}[N|Exp] + k_{exp}[N|Exp] \\ \frac{d[N|Exp]}{dt} &= k_2[N][Exp] - k_{-2}[N|Exp] - k_{exp}[N|Exp]\end{aligned}$$

The numerical solution of this set of ODEs, starting from a given initial species concentration and parameter values (e.g., rate constants for each reaction), provides the temporal evolution of the concentration of all involved species. One important point to take into account is the units of the rate constants: if the time is measured in seconds (s) and the concentrations in mol/L (molar, M), each equation will provide the speed of change of the reactants in units of M/s. therefore, for the equations to be consistent in terms of dimensions, the units of rate constants  $k_{-1}$ ,  $k_{-2}$ ,  $k_{imp}$  and  $k_{exp}$  have to be in  $s^{-1}$  (first order reactions), while whereas  $k_2$  and  $k_1$  are measured in  $(M \cdot s)^{-1}$  (second order reactions).

Figure 3A-C illustrates three different numerical solutions of the system, for a similar set of initial conditions, but using the parameter values listed as sets 1, 2 and 3 in Table 1, respectively. In all cases, the concentrations of the species change during the first seconds until they reach a steady state. Both  $[C]$  and  $[N]$  decrease while  $[C|Imp]$  and  $[N|Exp]$  increase (complexes are forming). The enzymes  $[Imp]$  and  $[Exp]$  also decrease as well due to complex formation. Due to the different parameter values used, three different steady states are reached: in Figure 3A the final concentration of  $[C]$  in the equilibrium is larger than the concentration of  $[N]$ , meaning that most protein is located at the cytoplasm for this values of the rate constants. The opposite scenario is shown in Figure 3C, where now the nuclear concentration is higher. Figure 3B corresponds to an intermediate situation, where parameters have been tuned to obtain an equilibrium condition where the concentration in the nucleus and in the cytoplasm is similar equivalent (case B) or smaller (case C). If we imagine an hypothetical situation where our molecule can be seen using immunofluorescence or by direct fusion with a fluorescence protein, case (A) would correspond to a cell that is brighter in the cytoplasm, case (C) would correspond to a cell with a brighter nuclei, and case (B) would correspond to a cell with homogeneous brightness. Note that the different cases were obtained by varying only the values of  $k_{imp}$  and  $k_{exp}$ , meaning that efficiency of the nuclear import and export processes ultimately controls the balance between nuclear and cytoplasmic configuration.

**Table 1.** Values of the constant rates for the different sets used in the simulations

| Rates     | Set 1                    | Set 2                     | Set 3                    | Set 4                    |
|-----------|--------------------------|---------------------------|--------------------------|--------------------------|
| $k_1$     | 500 (M·s) <sup>-1</sup>  | 500 (M·s) <sup>-1</sup>   | 500 (M·s) <sup>-1</sup>  | 50 (M·s) <sup>-1</sup>   |
| $k_{-1}$  | 0.15 s <sup>-1</sup>     | 0.15 s <sup>-1</sup>      | 0.15 s <sup>-1</sup>     | 1.5 s <sup>-1</sup>      |
| $k_2$     | 0.03 (M·s) <sup>-1</sup> | 0.036 (M·s) <sup>-1</sup> | 0.04 (M·s) <sup>-1</sup> | 0.03 (M·s) <sup>-1</sup> |
| $k_{-2}$  | 1000 s <sup>-1</sup>     | 1000 s <sup>-1</sup>      | 1000 s <sup>-1</sup>     | 1 s <sup>-1</sup>        |
| $k_{imp}$ | 0.1 s <sup>-1</sup>      | 0.1 s <sup>-1</sup>       | 0.1 s <sup>-1</sup>      | 0.3 s <sup>-1</sup>      |
| $k_{exp}$ | 0.026 s <sup>-1</sup>    | 0.023 s <sup>-1</sup>     | 0.01 s <sup>-1</sup>     | 0.3 s <sup>-1</sup>      |

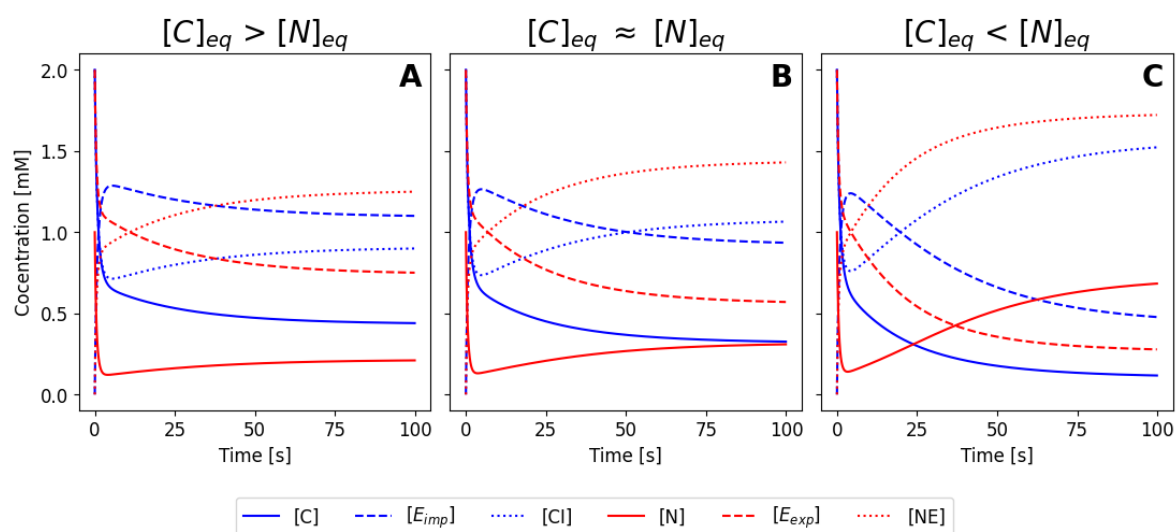


**Figure 3.** Simulation of the ODEs system. Three different sets 1, 2 and 3 (from Table 1) of rate constants are used for the different cases A, B and C, respectively. The initial condition for the species are  $[C](0) = [Imp](0) = [Exp](0) = 0.002$  M,  $[N](0) = 0.001$  M and  $[C|Imp](0) = [N|Exp](0) = 0$  M in all cases. The concentrations change during the first seconds until they reach a steady state:  $[C]$  in equilibrium is bigger (A), equivalent (B) or smaller than  $[N]$  in equilibrium. In general,  $[C]$ ,  $[N]$ ,  $[Imp]$  and  $[Exp]$  tend to decrease initially as  $[C|Imp]$  and  $[N|Exp]$  are formed.

#### *Simplifying the ODEs System Using the Mass Conservation Law*

To obtain simplifications and relations in the resulting ODEs system, it is often very useful to use the mass conservation law [64], stated by Antoine Lavoisier in 1789 [65]. Let's define a row matrix  $C$  of length  $n$ . This vector contains  $n$  constants  $C_1, C_2, \dots, C_n$  that will give the relationships between the concentrations of the species at any time. To obtain those relations, we have to use the following linear system:

$$C \cdot (B - A)^t = \vec{0} \quad (4)$$

We will get a set of  $n$  linear equations with  $n$  unknown variables. Using these equations, we must find the non-trivial relationship between all the  $C_j$  coefficients. For example, if the system we get is

$$C_1 - C_2 = 0 \quad (5)$$

$$C_2 - C_1 = 0 \quad (6)$$

$$C_3 + C_4 = 0 \quad (7)$$

so, we have a relation between the coefficients of  $x_1$  and  $x_2$  as  $C_1 = C_2$ . Also there is a relation between the coefficients of  $x_3$  and  $x_4$  as  $C_3 = -C_4$ . Given this values, the conservation law states that for a closed system, the following relation between the amounts of the reacts is always true:

$$\sum_{j=1}^n C_j \cdot [x_j] = \text{constant} \quad (8)$$

This way, if we substitute the relations obtained using equation 4 for the values of the coefficients  $C_j$ , the Equation 8 can be used to simplify the system of equations that describe a given system of interactions. To illustrate this with the previous example:



$$C_1[x_1] + C_2[x_2] + C_3[x_3] + C_4[x_4] = \text{constant}$$

using the relations calculated above becomes

$$C_1([x_1] + [x_2]) + C_3([x_3] - [x_4]) = \text{constant}$$

This is true for all values of  $C_1$  and  $C_3$ . So, if we set  $C_1 = 1$  and  $C_3 = 0$  we obtain the following the relation

$$[x_1] + [x_2] = \text{constant} \quad (9)$$

while if we set  $C_1 = 0$  and  $C_3 = 1$  we obtain the following the relation

$$[x_3] - [x_4] = \text{constant} \quad (10)$$

Now, it is important to realize that if this relation between the amounts of the species involved in Equations 9-10 is true at all times, it means that it is also true at the initial time point ( $t=0$ ). This is useful because we normally know the initial conditions of the system. This way, we can write:

$$\begin{aligned} [x_1] + [x_2] &= [x_1]_{t=0} + [x_2]_{t=0} \\ [x_3] - [x_4] &= [x_3]_{t=0} - [x_4]_{t=0} \end{aligned}$$

which can be used to calculate one of the variables as a function of the other, plus or minus some constant values that are known. This way:

$$[x_2] = [x_1]_{t=0} + [x_2]_{t=0} - [x_1]$$

$$[x_4] = [x_3] - [x_3]_{t=0} - [x_4]_{t=0}$$

Going back to our nuclear translocation model, in the previous step we dealt with a system composed of six ODEs. In these these type of systems, some equations are redundant or the dynamics of change is too fast or too slow. In this conditions, simplification of the system is a good way to produce a more transparent and easier to interpret set of equations, with less free parameters. In this case, we will start by applying the mass conservation law to reduce the number of equations from 6 to 4. We start again by defining a row vector  $C$  with six constants ( $C_1, \dots, C_6$  -one per species) and calculate expression 4 for this particular system:

$$C \cdot (B - A)^t = \vec{0}$$

$$(C_1 \ C_2 \ C_3 \ C_4 \ C_5 \ C_6) \begin{pmatrix} -1 & 1 & 0 & 0 & 0 & 1 \\ -1 & 1 & 0 & 0 & 1 & 0 \\ 1 & -1 & 0 & 0 & -1 & 0 \\ 0 & 0 & -1 & 1 & 1 & 0 \\ 0 & 0 & -1 & 1 & 0 & 1 \\ 0 & 0 & 1 & -1 & 0 & -1 \end{pmatrix} = \vec{0}$$

This relation gives us linear system of equations. Removing the independent equations and simplifying, we reach the following equivalences:

$$\begin{aligned}C_1 + C_2 &= C_3 \\C_4 + C_5 &= C_6 \\C_1 &= C_4\end{aligned}$$

The mass conservation law states that the following expression has a constant value over time:

$$\begin{aligned}C_1[C] + C_2[Imp] + C_3[C|Imp] + ... \\+ C_4[N] + C_5[Exp] + C_6[N|Exp] = constant\end{aligned}$$

which, after applying the relations between the coefficients above gives us:

$$\begin{aligned}C_1[C] + C_2[Imp] + (C_1 + C_2)[C|Imp] + ... \\+ C_1[N] + C_5[Exp] + (C_1 + C_5)[N|Exp] = constant\end{aligned}$$

So, we have three independent variables, and the previous equation is true for all values of the three. This way, following the same rationale as in the example, we set each one to a value of 1, while the others are set equal to 0. This way we obtain the three constant relations as:

$$\begin{aligned}C_1([C] + [C|Imp] + [N] + [N|Exp]) &= constant \\C_2([Imp] + [C|Imp]) &= constant \\C_5([Exp] + [N|Exp]) &= constant\end{aligned}$$

In particular, these relations are true at all time points, therefore they are true at the initial time point. This way, if we set  $C_1 = C_2 = C_5 = 1$  and the constant values as the value at  $t = 0$  (initial conditions) we obtain

$$\begin{aligned}[C] + [C|Imp] + [N] + [N|Exp] &= [C](0) + [C|Imp](0) \\&\quad + [N](0) + [N|Exp](0) \\[Imp] + [C|Imp] &= [Imp](0) + [C|Imp](0) \\[Exp] + [N|Exp] &= [Exp](0) + [N|Exp](0)\end{aligned}$$

The first relation corresponds to the fact that total amount of Smad in all possible configurations (nuclear, cytoplasmic, alone or in complex) has to remain constant. The second and third relations corresponds to the fact that the total amount of Import and Export proteins has to remain constant. One additional simplification can be introduced, taking into account that at the initial time point, there is no complexes, since we start with all proteins as monomers and monitor their interaction. This way, we can assume  $[C|Imp](0) = [N|Exp](0) = 0$ , so, the relations result in:

$$\begin{aligned}[C] + [C|Imp] + [N] + [N|Exp] &= [C](0) + [N](0) \\[Imp] + [C|Imp] &= [Imp](0) \\[Exp] + [N|Exp] &= [Exp](0)\end{aligned}$$

The next step is to calculate the concentrations of some reactants as a function of the other. In this case, since we often focus on the amounts of the R-Smads and not in the amount of Import and Export proteins, it makes sense that we use organize the relations in such a way that we eliminate the variables  $[Imp]$  and  $[Exp]$ :

$$\begin{aligned}[Imp] &= [Imp](0) - [C|Imp] \\ [Exp] &= [Exp](0) - [N|Exp]\end{aligned}$$

Finally, we substitute these relations in the system of ODEs, as:

$$\begin{aligned}\frac{d[C]}{dt} &= -k_1[C]([Imp](0) - [C|Imp]) + \dots \\ &\quad + k_{-1}[C|Imp] + k_{exp}[N|Exp] \\ \frac{d[C|Imp]}{dt} &= k_1[C]([Imp](0) - [C|Imp]) - \dots \\ &\quad - k_{-1}[C|Imp] - k_{imp}[C|Imp] \\ \frac{d[N]}{dt} &= -k_2[N]([Exp](0) - [N|Exp]) + \dots \\ &\quad + k_{-2}[N|Exp] + k_{imp}[C|Imp] \\ \frac{d[N|Exp]}{dt} &= k_2[N]([Exp](0) - [N|Exp]) - \dots \\ &\quad - k_{-2}[N|Exp] - k_{exp}[N|Exp]\end{aligned}$$

which gives a more simple set of 4 ODEs. Numerical integration of this set will give you the temporal evolution of  $[C]$ ,  $[N]$  and the complexes  $[C|Imp]$  and  $[N|Exp]$ . If needed, the temporal evolution of the enzymes can be simply calculated as  $[Imp](t) = [Imp](0) - [C|Imp](t)$  and  $[Exp](t) = [Exp](0) - [N|Exp](t)$ . This means that we can calculate the concentration of all six species over time just solving four ODEs instead of the six that we obtained initially. Numerical solution of these four ODEs is shown in Figure 4, for the same parameters and initial conditions as before.

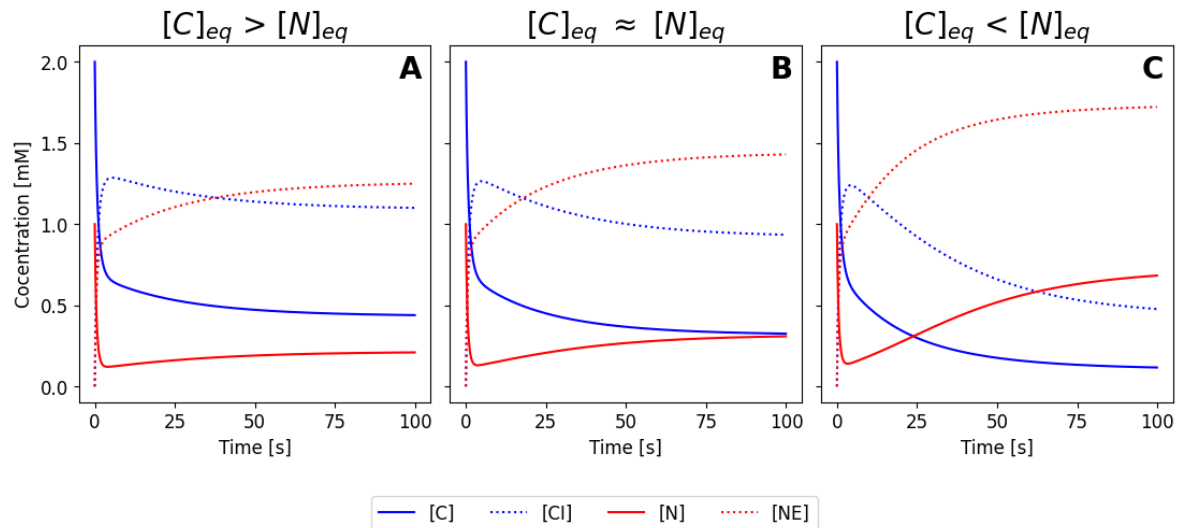


**Figure 4.** Simulation of the ODEs system after using the mass conservation law. The simulation parameters are the same as those in Figure 3. The curves shown in this figure only correspond to the solution of the ODEs, which are the same as in Figure 3. The  $[Imp]$  and  $[Exp]$  curves are not shown, but they have the same behaviour as in Figure 3.

### Non-Dimensionalization of the Model

To increase the predictive capability of the model, a common potential approach is to remove the dimensions of the concentrations and the time, expressing both of them as a factor in an appropriate scale for the system of study. In this type of adimensional systems, it is easier to compare parameter values and to interpret the results from the ODEs, since they will show relative changes from a maximum to a minimum value, instead of absolute values.

In order to make the concentrations non-dimensional, we will rewrite the model in terms of new variables with no units. This is achieved by multiplying each equation by a scaling factor (with concentration units), in such a way that now the concentration of the species  $[X]$  (dimensional) will now be represented by  $[\tilde{X}]$  (adimensional), related via the scaling factor  $X_0$  [59]:

$$[X](t) = [\tilde{X}](t) \cdot X_0 \quad (11)$$

The scaling factor for each species is chosen as its maximum value. This way, the non-dimensional species concentration  $[\tilde{X}]$  associated will fall between the range  $[0, 1]$ . The maximum amount of molecules in the cytoplasm that we can have is  $[C](0)$ , and as one molecule of  $C$  can only produce one molecule of  $N$ , then the maximum value for the latter is  $[C](0)$  as well (supposing that  $[N](0) = 0$ ). In the case of the enzymes, the maximum concentration for each will be also its initial concentration. For the scaling factor of the complexes  $C|Imp$  and  $N|Exp$ , we cannot use their initial concentration as it is zero. Therefore, we must find which is the maximum concentration that they can reach over time ( $[C|Imp]_{max}$  and  $[N|Exp]_{max}$ ), which will happen at a particular time point  $t = t_{max}$  (this value of the time can be different for  $[C|Imp]$  and  $[N|Exp]$ ):

$$\begin{aligned} [C|Imp]_{max} &= \frac{k_1[C](t_{max})[Imp](0)}{k_1 \cdot [C](t_{max}) + k_{-1} + k_{imp}} \\ [N|Exp]_{max} &= \frac{k_2[N](t_{max})[Exp](0)}{k_2 \cdot [N](t_{max}) + k_{-2} + k_{exp}} \end{aligned}$$

Next, these expressions can be further simplified by making some assumptions. As the dynamics of the complexes are very fast,  $k_2$  and  $k_1$  are much larger than the other rate constants. Considering that, we can assume that  $k_{-1} = k_{imp} = k_{-2} = k_{exp} = 0$ , and therefore:

$$\begin{aligned} [C|Imp]_{max} &\approx [Imp](0) \\ [N|Exp]_{max} &\approx [Exp](0) \end{aligned}$$

Then, the new non-dimensional variables are defined as:

$$\begin{aligned} [\tilde{C}] &= \frac{[C]}{[C](0)} \\ [I\tilde{m}p] &= \frac{[Imp]}{[Imp](0)} \\ [C|\tilde{I}mp] &= \frac{[C|Imp]}{[Imp](0)} \\ [\tilde{N}] &= \frac{[N]}{[N](0)} \\ [E\tilde{x}p] &= \frac{[Exp]}{[Exp](0)} \\ [N|\tilde{E}xp] &= \frac{[N|Exp]}{[Exp](0)} \end{aligned}$$

Substituting these values in the ODEs system, we obtain the new partially non-dimensional ODEs system:

$$\begin{aligned}
\frac{d[\tilde{C}]}{dt} &= k_1[\tilde{C}][Imp](0)([C|\tilde{Imp}] - 1) + \dots \\
&\quad + k_{-1} \frac{[Imp](0)}{[C](0)} [C|\tilde{Imp}] + k_{exp} \frac{[Exp](0)}{[C](0)} [N|\tilde{Exp}] \\
\frac{d[C|\tilde{Imp}]}{dt} &= k_1[\tilde{C}][C](0)(1 - [C|\tilde{Imp}]) - \dots \\
&\quad - (k_{-1} + k_{exp})[C|\tilde{Imp}] \\
\frac{d[\tilde{N}]}{dt} &= k_2[\tilde{N}][Exp](0)([N|\tilde{Exp}] - 1) + \dots \\
&\quad + k_{-2} \frac{[Exp](0)}{[N](0)} [N|\tilde{Exp}] + k_{imp} \frac{[Imp](0)}{[N](0)} [C|\tilde{Imp}] \\
\frac{d[N|\tilde{Exp}]}{dt} &= k_2[\tilde{N}][N](0)(1 - [N|\tilde{Exp}]) - \dots \\
&\quad - (k_{-2} + k_{imp})[N|\tilde{Exp}] \\
[I\tilde{mp}](t) &= 1 - [C|\tilde{Imp}](t) \\
[E\tilde{x}p](t) &= 1 - [N|\tilde{Exp}](t)
\end{aligned}$$

It is important to highlight that the mass conservation law in this case is different from the dimensional system. Calculations in the case are not shown, but they are analogous to those in the previous case.

To remove the dimensionalization in time, a scaling factor  $t_0$  is required in order to define a new dimensionless time variable  $\tau$  as:

$$\tau = \frac{t}{t_0}$$

In any system, we have several reaction rate constants that have different values. To obtain the scaling factor, one option is to choose the fastest one, as then the dimensionless time will be a factor indicating “how many times the fastest reaction has taken place”. In any case, we can rewrite our ODEs system, taking into account that,

$$\frac{d}{dt} = \frac{1}{t_0} \frac{d}{d\tau}$$

and obtain:

$$\begin{aligned}
\frac{1}{t_0} \frac{d[\tilde{C}]}{d\tau} &= k_1[\tilde{C}][Imp](0)([C|\tilde{Imp}] - 1) + \dots \\
&\quad + k_{-1} \frac{[Imp](0)}{[C](0)} [C|\tilde{Imp}] + k_{exp} \frac{[Exp](0)}{[C](0)} [N|\tilde{Exp}] \\
\frac{1}{t_0} \frac{d[C|\tilde{Imp}]}{d\tau} &= k_1[\tilde{C}][C](0)(1 - [C|\tilde{Imp}]) - \dots \\
&\quad - (k_{-1} + k_{exp})[C|\tilde{Imp}] \\
\frac{1}{t_0} \frac{d[\tilde{N}]}{d\tau} &= k_2[\tilde{N}][Exp](0)([N|\tilde{Exp}] - 1) + \dots \\
&\quad + k_{-2} \frac{[Exp](0)}{[N](0)} [N|\tilde{Exp}] + k_{imp} \frac{[Imp](0)}{[N](0)} [C|\tilde{Imp}] \\
\frac{1}{t_0} \frac{d[N|\tilde{Exp}]}{d\tau} &= k_2[\tilde{N}][N](0)(1 - [N|\tilde{Exp}]) - \dots \\
&\quad - (k_{-2} + k_{imp})[N|\tilde{Exp}] \\
[I\tilde{mp}](\tau) &= 1 - [C|\tilde{Imp}](\tau) \\
[E\tilde{x}p](\tau) &= 1 - [N|\tilde{Exp}](\tau)
\end{aligned}$$



In our example, let's suppose  $k_2$  is the fastest rate (which is a biologically plausible assumption). As  $k_2$  is measured in  $(\text{M}\cdot\text{s})^{-1}$ , it cannot be the scaling factor itself because then  $\tau$  will have dimensions of  $\text{M}\cdot\text{s}^2$ . Looking at the simplified ODEs system using the mass conservation law, we can see that this rate  $k_2$  appears multiplied by a constant,  $[\text{Exp}](0)$ , measured in  $\text{M}$ . The product  $[\text{Exp}](0) \cdot k_2$  is measured in  $\text{s}^{-1}$ , so we can choose our scaling factor to be:

$$t_0 = \frac{1}{k_2 \cdot [\text{Exp}](0)} \rightarrow \tau = k_2 \cdot [\text{Exp}](0) \cdot t$$

Numerical integration of this adimensional version for the same parameters is now shown in Figure 5, where vertical axis now moves from 0 to 1 and the horizontal axis represents multiples of the  $t_0$  value.

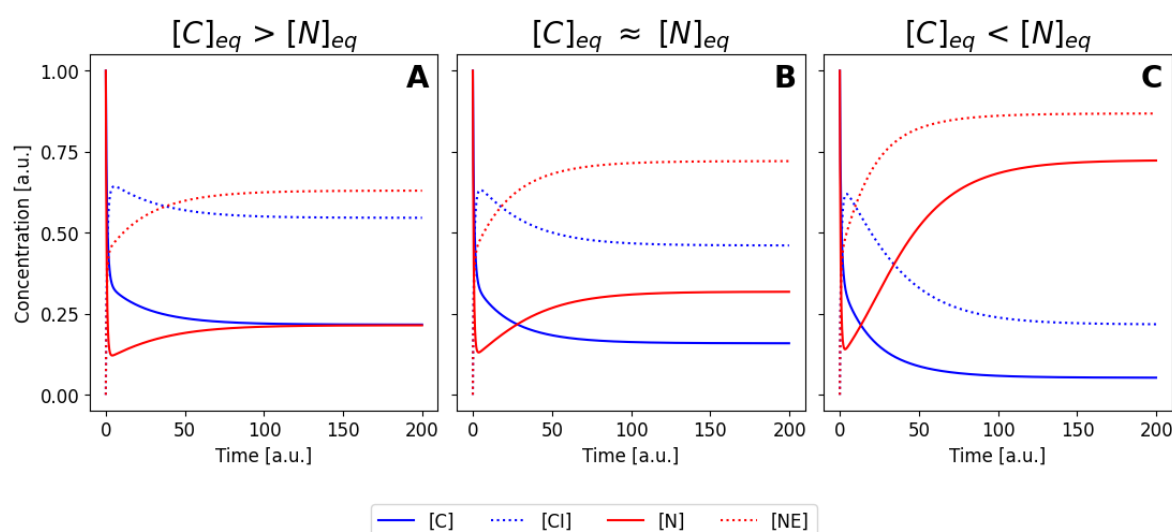


**Figure 5.** Simulation of the ODEs system after using the non-dimensionalization. The same rate constants and initial conditions as in Figure 3 have been used for all the insets. Note that the concentrations are ranged in  $[0, 1]$ , and during the simulation the curves indicate the present fraction of the initial concentration of each species in the system.

### Pseudo-Steady State Approximation

So far we have an ODEs system with 4 coupled equations. Although in this case the numerical solution of this system is relatively easy to achieve, this might not be the case in any other systems. To further simplify our mathematical model, a common approach is to take advantage of the so-called pseudo-steady state approximation.

A biologically acceptable approximation will be to consider that the dynamics of the intermediate complexes are very fast, compared with the rest of the species. This means that the translocation processes ( $\text{C|Imp}$  and  $\text{N|Exp}$  moving from one compartment to another via diffusion or another active process, plus their disassembly) are slow compared to the association and dissociation reactions ( $\text{C|Imp}$  and  $\text{N|Exp}$  formation and disassembly). Mathematically, this translates in  $k_{\text{imp}}$  and  $k_{\text{exp}}$  being much smaller than the rest of the rate constants, and thus we can consider that

$$\frac{d[\text{C|Imp}]}{dt} = \frac{d[\text{N|Exp}]}{dt} = 0$$

This assumption is known as Michaelis-Menten approximation [59], in which the concentration of the enzymes and complexes are considered to be in equilibrium while  $[\text{C}]$  and  $[\text{N}]$  change rapidly. With this mathematical condition, we can then obtain the concentration of the complexes over time as:

$$[C|Imp](t) = \frac{k_1[C](t)[Imp](0)}{k_1[C](t) + k_{-1} + k_{imp}}$$

$$[N|Exp](t) = \frac{k_2[N](t)[Exp](0)}{k_2[N](t) + k_{-2} + k_{exp}}$$

With this definitions, then the new simplified system that gives the concentration of all the species over time is:

$$\begin{aligned} \frac{d[C]}{dt} &= -k_1[C][Imp](0) + \dots \\ &+ (k_1[C] + k_{-1}) \frac{k_1[C][Imp](0)}{k_1[C] + k_{-1} + k_{imp}} + \dots \\ &+ k_{exp} \frac{k_2[N][Exp](0)}{k_2[N] + k_{-2} + k_{exp}} \\ \frac{d[N]}{dt} &= -k_2[N][Exp](0) + \dots \\ &+ (k_2[N] + k_{-2}) \frac{k_2[N][Exp](0)}{k_2[N] + k_{-2} + k_{exp}} + \dots \\ &+ k_{imp} \frac{k_1[C][Imp](0)}{k_1[C] + k_{-1} + k_{imp}} \end{aligned}$$

which just has two coupled ODEs. Lastly, using the definition of the Michaelis-Menten constant for each of the two processes ( $C/Imp$  and  $N/Exp$ ), we can rewrite the ODEs as:

$$\begin{aligned} \frac{d[C]_{MM}}{dt} &= k_{exp} \frac{[Exp](0)[N]}{K_N + [N]} - k_{imp} \frac{[Imp](0)[C]}{K_C + [C]} \\ \frac{d[N]_{MM}}{dt} &= k_{imp} \frac{[Imp](0)[C]}{K_C + [C]} - k_{exp} \frac{[Exp](0)[N]}{K_N + [N]} \end{aligned}$$

with:

$$\begin{aligned} K_C &= \frac{k_{imp} + k_{-1}}{k_1} \\ K_N &= \frac{k_{exp} + k_{-2}}{k_2} \end{aligned}$$

Now, we can compare the initial system with the pseudo-state approximation system that we have just obtained. As shown in Figure 6, the approximation is not valid for the values of the rates of the set 1 (Table 1), but it is for the values of set 4. The rate constants for the system must fulfill the approximation assumptions in order to be able to use the approximation.

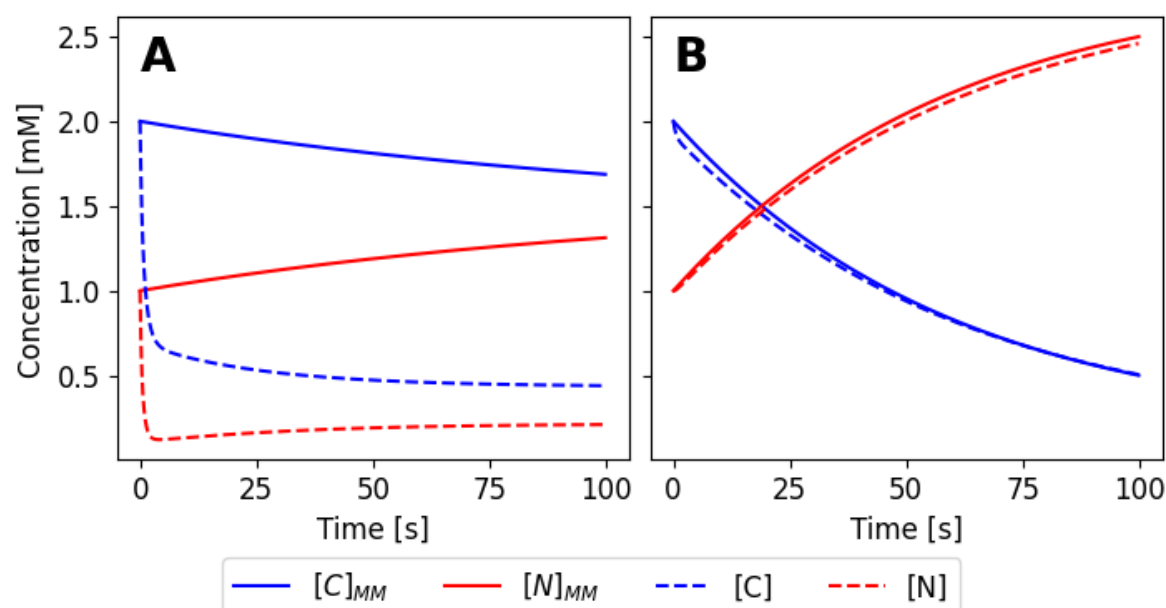


**Figure 6.** Comparison of the raw model and the pseudo-steady state approximation model. The concentration of the C and N molecules are shown as dashed lines for the original ODEs ( $[C]$  and  $[N]$ ) and as solid lines for the pseudo-state approximation (Michaelis-Menten,  $[C]_{MM}$  and  $[N]_{MM}$ ). In both insets, the initial concentration values are the same as in Figure 3. The rate constants used in A and B are set 1 and 4 (from Table 1), respectively. For case A, there is a considerable discrepancy between the approximation (solid curves) and the original system (dashed curves). When the rate constants are chosen in a way that the approximation assumptions are fulfilled (set 4), the steady-state approximation becomes valid and can be used to simplify the analysis of the system.

## Conclusions

Here we presented a comprehensive revision on how the different compartments in a cell are often utilized as physical barriers to modulate the biochemical processes that shape the response of cells to external stimuli. The TFG $\beta$  is often viewed as an almost linear cascade, where events at the receptor level correspond to direct phosphorylation and activation of transcription factors. This oversimplified view leaves out important processes that can fully dictate the response, such as regulation via compartmentalization of the R-Smads, that are actively maintained in and out of the nucleus depending on their activation state. In principle, inactive unphosphorylated R-Smads do not form complexes and do not bind to DNA, so the fact that there is an extra layer that keeps this inactive proteins from entering the nucleus seems unnecessary. But we know from experience that everything that happens inside the cells serves often many purposes. Therefore, this biophysical regulation at least adds an extra safety layer that prevents such important proteins to wrongly activate expression of their targets when not needed. We believe that this is just one of many ways that the physical aspects of the cells and organelles shape influence biological responses, and perhaps some still waiting to be discovered and studied. Physics and biophysics have already helped to understand many of the most important aspects of how living systems operate, and for sure will play a central role in future discoveries.

**Author Contributions:** ANH, DP and DGM performed research and wrote the manuscript. DP performed numerical simulations. DMG and ANH provided funding.

**Acknowledgments:** We acknowledge all CBMSO (Centre for Molecular Biology Severo Ochoa, CSIC-UAM) facilities. This work was supported by grants from the Ministerio de Ciencia e Innovación, Spain (RTI2018-096953-B-I00, PID2022-140421NB-I00, PDC2022-133147-I00, an FPI fellowship. Institutional fellowships to the IFIMAC (María de Maeztu unit of excellence) and CBMSO (Severo Ochoa). ML acknowledges a Margarita Salas fellowship from the Ministerio de Ciencia e Innovación (CA4/RSUE/2022-00236).

**Conflicts of Interest:** Authors declare no Competing Intensest.

## References

- Heldin, C.H.; Moustakas, A. Signaling Receptors for TGF-beta Family Members. *Cold Spring Harbor Perspectives in Biology* **2016**, *8*, a022053. doi:10.1101/cshperspect.a022053.
- Zhong, Q.; Xiao, X.; Qiu, Y.; Xu, Z.; Chen, C.; Chong, B.; Zhao, X.; Hai, S.; Li, S.; An, Z.; Dai, L. Protein posttranslational modifications in health and diseases: Functions, regulatory mechanisms, and therapeutic implications. *MedComm* **2023**, *4*, Not available. doi:10.1002/mco2.261.
- Editorial : Ebb and Tide of Glucokinase FRANZ M . MATSCHINSKY. 2008.
- Jetton, T.L.; Shiota, M.; Knobel, S.M.; Piston, D.W.; Cherrington, A.D.; Magnuson, M.A. Substrate-induced Nuclear Export and Peripheral Compartmentalization of Hepatic Glucokinase Correlates with Glycogen Deposition. *Journal of Diabetes Research* **2001**, *2*, 173–186. doi:10.1155/edr.2001.173.
- Erb, T.J.; Zarzycki, J. A short history of RubisCO: the rise and fall (?) of Nature's predominant CO<sub>2</sub> fixing enzyme. *Current Opinion in Biotechnology* **2018**, *49*, 100–107. Food biotechnology • Plant biotechnology, doi:https://doi.org/10.1016/j.copbio.2017.07.017.
- Amritkar, K.; Cuevas-Zuñiría, B.; Kacar, B. Ancestral structure prediction reveals the conformational impact of the RuBisCO small subunit across time. *bioRxiv* **2024**.
- Ruiz-Herrero, T.; Estrada, J.; Guantes, R.; Míguez, D.G. A Tunable Coarse-Grained Model for Ligand-Receptor Interaction. *PLoS Computational biology* **2013**, *9*, e1003274–e1003274.
- Doldán-Martelli, V.; Míguez, D.G. Synergistic Interaction between Selective Drugs in Cell Populations Models. *PLOS ONE* **2015**, *10*, e0117558. doi:10.1371/journal.pone.0117558.
- Doldán-Martelli, V.; Guantes, R.; Míguez, D.G. A mathematical model for the rational design of chimeric ligands in selective drug therapies. *CPT: pharmacometrics & systems pharmacology* **2013**, *2*, e26–e26. doi:10.1038/psp.2013.2.
- Míguez, D.G. The role of asymmetric binding in ligand-receptor systems with 1:2 interaction ratio. *Biophysical Chemistry* **2010**, *148*, 74–81. doi:10.1016/j.bpc.2010.02.012.
- Xu, X.; Zheng, L.; Yuan, Q.; Zhen, G.; Crane, J.L.; Zhou, X.; Cao, X. Transforming growth factor-β in stem cells and tissue homeostasis. *Bone Research* **2018**, *6*, 2. doi:10.1038/s41413-017-0005-4.
- Papanikolaou, S.; Vourda, A.; Sygdelos, S.; Gyftopoulos, K. Cell Plasticity and Prostate Cancer: The Role of Epithelial–Mesenchymal Transition in Tumor Progression, Invasion, Metastasis and Cancer Therapy Resistance. *Cancers* **2021**, *13*, 2795. doi:10.3390/cancers13112795.
- Derynck, R.; Budi, E.H. Specificity, versatility, and control of TGF-beta family signaling. *Science Signaling* **2019**, *12*, eaav5183. doi:10.1126/scisignal.aav5183.
- Deng, Z.; Fan, T.; Xiao, C.; Tian, H.; Zheng, Y.; Li, C.; He, J. TGF-beta signaling in health, disease and therapeutics. *Signal Transduction and Targeted Therapy* **2024**, *9*, 61. doi:10.1038/s41392-024-01764-w.
- Goebel, E.J.; Hart, K.N.; McCoy, J.C.; Thompson, T.B. Structural biology of the TGFβ family. *Experimental Biology and Medicine* **2019**, *244*, 1530–1546. doi:10.1177/1535370219880894.
- Tzavlaki, K.; Moustakas, A. TGF-beta Signaling. *Biomolecules* **2020**, *10*, 487. doi:10.3390/biom10030487.
- Huang, T.; David, L.; Mendoza, V.; Yang, J.; De, K.; Sun, L.; Fang, J.; Wrana, J.L.; Hinck, A.P. TGF-beta signalling is mediated by two autonomously functioning TBRI:TBRII pairs. *The EMBO Journal* **2011**, *30*, 1263–1276. doi:10.1038/emboj.2011.54.
- Mitchell, H.; Choudhury, A.; Pagano, R.E.; Leof, E.B. Ligand-dependent and -independent Transforming Growth Factor-β Receptor Recycling Regulated by Clathrin-mediated Endocytosis and Rab11. *Molecular Biology of the Cell* **2004**, *15*, 4166–4178. doi:10.1091/mbc.e04-03-0245.
- Derynck, R.; Zhang, Y.E. Smad-dependent and Smad-independent pathways in TGF-β family signalling. *Nature* **2003**, *425*, 577–584. doi:10.1038/nature02006.
- Kim, M.S.; Jin, W. TrkB-Induced Inhibition of R-SMAD/SMAD4 Activation is Essential for TGF-beta-Mediated Tumor Suppressor Activity. *Cancers* **2020**, *12*, 1048. doi:10.3390/cancers12041048.
- Budi, E.H.; Duan, D.; Derynck, R. Transforming Growth Factor-β Receptors and Smads: Regulatory Complexity and Functional Versatility. *Trends in Cell Biology* **2017**, *27*, 658–672. doi:10.1016/j.tcb.2017.04.005.
- Miyazawa, K.; Miyazono, K. Regulation of TGF-beta Family Signaling by Inhibitory Smads. *Cold Spring Harbor Perspectives in Biology* **2017**, *9*, a022095. doi:10.1101/cshperspect.a022095.

23. Aykul, S.; Maust, J.; Thamilselvan, V.; Floer, M.; Martinez-Hackert, E. Smad2/3 Activation Regulates Smad1/5/8 Signaling via a Negative Feedback Loop to Inhibit 3T3-L1 Adipogenesis. *International Journal of Molecular Sciences* **2021**, *22*, 8472. doi:10.3390/ijms22168472.
24. Baburajendran, N.; Jauch, R.; Tan, C.Y.Z.; Narasimhan, K.; Kolatkar, P.R. Structural basis for the cooperative DNA recognition by Smad4 MH1 dimers. *Nucleic Acids Research* **2011**, *39*, 8213–8222. doi:10.1093/nar/gkr500.
25. Xin, X.; Cheng, X.; Zeng, F.; Xu, Q.; Hou, L. The Role of TGF-beta/SMAD Signaling in Hepatocellular Carcinoma: from Mechanism to Therapy and Prognosis. *International Journal of Biological Sciences* **2024**, *20*, 1436–1451. doi:10.7150/ijbs.89568.
26. Hata, A.; Chen, Y.G. TGF-beta Signaling from Receptors to Smads. *Cold Spring Harbor Perspectives in Biology* **2016**, *8*, a022061. doi:10.1101/cshperspect.a022061.
27. Xu, F.; Liu, C.; Zhou, D.; Zhang, L. TGF-beta/SMAD Pathway and Its Regulation in Hepatic Fibrosis. *Journal of Histochemistry & Cytochemistry* **2016**, *64*, 157–167. doi:10.1369/0022155415627681.
28. Bai, H.; Lester, G.M.; Petishnok, L.; Dean, D. Cytoplasmic transport and nuclear import of plasmid DNA. *Bioscience Reports* **2017**, *37*, BSR20160616. doi:10.1042/BSR20160616.
29. Schmierer, B.; Hill, C.S. Kinetic Analysis of Smad Nucleocytoplasmic Shuttling Reveals a Mechanism for Transforming Growth Factor  $\beta$ -Dependent Nuclear Accumulation of Smads. *Molecular and Cellular Biology* **2005**, *25*, 9845–9858. doi:10.1128/MCB.25.22.9845-9858.2005.
30. Hill, C.S. Nucleocytoplasmic shuttling of Smad proteins. *Cell Research* **2009**, *19*, 36–46. doi:10.1038/cr.2008.325.
31. Paci, G.; Caria, J.; Lemke, E.A. Cargo transport through the nuclear pore complex at a glance. *Journal of Cell Science* **2021**, *134*, jcs247874. doi:10.1242/jcs.247874.
32. Otsuka, S.; Ellenberg, J. Mechanisms of nuclear pore complex assembly – two different ways of building one molecular machine. *FEBS Letters* **2018**, *592*, 475–488. doi:10.1002/1873-3468.12905.
33. Timney, B.L.; Raveh, B.; Mironska, R.; Trivedi, J.M.; Kim, S.J.; Russel, D.; Wente, S.R.; Sali, A.; Rout, M.P. Simple rules for passive diffusion through the nuclear pore complex. *Journal of Cell Biology* **2016**, *215*, 57–76. doi:10.1083/jcb.201601004.
34. Oka, M.; Yoneda, Y. Importin  $\alpha$ : functions as a nuclear transport factor and beyond. *Proceedings of the Japan Academy, Series B* **2018**, *94*, 259–274. doi:10.2183/pjab.94.018.
35. Yang, Y.; Guo, L.; Chen, L.; Gong, B.; Jia, D.; Sun, Q. Nuclear transport proteins: structure, function and disease relevance. *Signal Transduction and Targeted Therapy* **2023**, *8*, 425. doi:10.1038/s41392-023-01649-4.
36. Kurisaki, A.; Kose, S.; Yoneda, Y.; Heldin, C.H.; Moustakas, A. Transforming Growth Factor- $\beta$  Induces Nuclear Import of Smad3 in an Importin- $\beta$ 1 and Ran-dependent Manner. *Molecular Biology of the Cell* **2001**, *12*, 1079–1091. doi:10.1091/mbc.12.4.1079.
37. Chen, X.; Xu, L. Mechanism and Regulation of Nucleocytoplasmic Trafficking of Smad. *Cell & Bioscience* **2011**, *1*, 40. doi:10.1186/2045-3701-1-40.
38. Kırılı, K.; Karaca, S.; Dehne, H.J.; Samwer, M.; Pan, K.T.; Lenz, C.; Urlaub, H.; Görlich, D. A deep proteomics perspective on CRM1-mediated nuclear export and nucleocytoplasmic partitioning. *eLife* **2015**, *4*, e11466. doi:10.7554/eLife.11466.
39. Abdel Mouti, M.; Pauklin, S. TGFBI/INHBA Homodimer/Nodal-SMAD2/3 Signaling Network: A Pivotal Molecular Target in PDAC Treatment. *Molecular Therapy* **2021**, *29*, 920–936. doi:10.1016/j.ymthe.2021.01.002.
40. Watanabe, M.; Masuyama, N.; Fukuda, M.; Nishida, E. Regulation of intracellular dynamics of Smad4 by its leucine-rich nuclear export signal. *EMBO reports* **2000**, *1*, 176–182. doi:10.1093/embo-reports/kvd029.
41. Dai, F.; Lin, X.; Chang, C.; Feng, X.H. Nuclear Export of Smad2 and Smad3 by RanBP3 Facilitates Termination of TGF- $\beta$  Signaling. *Developmental Cell* **2009**, *16*, 345–357. doi:10.1016/j.devcel.2009.01.022.
42. Xu, L.; Kang, Y.; Çöl, S.; Massagué, J. Smad2 Nucleocytoplasmic Shuttling by Nucleoporins CAN/Nup214 and Nup153 Feeds TGF $\beta$  Signaling Complexes in the Cytoplasm and Nucleus. *Molecular Cell* **2002**, *10*, 271–282. doi:10.1016/s1097-2765(02)00586-5.
43. Kofler, M.; Kapus, A. Nuclear Import and Export of YAP and TAZ. *Cancers* **2023**, *15*, 4956. doi:10.3390/cancers15204956.
44. Kurisaki, A.; Kurisaki, K.; Kowanetz, M.; Sugino, H.; Yoneda, Y.; Heldin, C.H.; Moustakas, A. The Mechanism of Nuclear Export of Smad3 Involves Exportin 4 and Ran. *Molecular and Cellular Biology* **2006**, *26*, 1318–1332. doi:10.1128/mcb.26.4.1318-1332.2006.



45. Song, R.; Tikoo, S.; Jain, R.; Pinello, N.; Au, A.Y.M.; Nagarajah, R.; Porse, B.; Rasko, J.E.J.; J.-L. Wong, J. Dynamic intron retention modulates gene expression in the monocytic differentiation pathway. *Immunology* **2022**, *165*, 274–286. doi:10.1111/imm.13435.
46. Pierreux, C.E.; Nicolás, F.J.; Hill, C.S. Transforming Growth Factor  $\beta$ -Independent Shuttling of Smad4 between the Cytoplasm and Nucleus. *Molecular and Cellular Biology* **2000**, *20*, 9041–9054. doi:10.1128/MCB.20.23.9041-9054.2000.
47. Zou, M.L.; Chen, Z.H.; Teng, Y.Y.; Liu, S.Y.; Jia, Y.; Zhang, K.W.; Sun, Z.L.; Wu, J.J.; Yuan, Z.D.; Feng, Y.; Li, X.; Xu, R.S.; Yuan, F.L. The Smad Dependent TGF- $\beta$  and BMP Signaling Pathway in Bone Remodeling and Therapies. *Frontiers in Molecular Biosciences* **2021**, *8*, 593310. doi:10.3389/fmolb.2021.593310.
48. Warmflash, A.; Zhang, Q.; Sorre, B.; Vonica, B.; Brivanlou, A.H. Dynamics of TGF- $\beta$  signaling reveal adaptive and pulsatile behaviors reflected in the nuclear localization of transcription factor Smad4. *Proceedings of the National Academy of Sciences* **2012**, *109*. doi:10.1073/pnas.1207607109.
49. Li, Y.; Luo, W.; Yang, W. Nuclear Transport and Accumulation of Smad Proteins Studied by Single-Molecule Microscopy. *Biophysical Journal* **2018**, *114*, 2243–2251. doi:10.1016/j.bpj.2018.03.018.
50. Nicolás, F.J.; De Bosscher, K.; Schmierer, B.; Hill, C.S. Analysis of Smad nucleocytoplasmic shuttling in living cells. *Journal of Cell Science* **2004**, *117*, 4113–4125. doi:10.1242/jcs.01289.
51. Zi, Z.; Feng, Z.; Chapnick, D.A.; Dahl, M.; Deng, D.; Klipp, E.; Moustakas, A.; Liu, X. Quantitative analysis of transient and sustained transforming growth factor- $\beta$  signaling dynamics. *Molecular Systems Biology* **2011**, *7*, 492. doi:10.1038/msb.2011.22.
52. Sorre, B.; Warmflash, A.; Brivanlou, A.; Siggia, E. Encoding of Temporal Signals by the TGF- $\beta$  Pathway and Implications for Embryonic Patterning. *Developmental Cell* **2014**, *30*, 334–342. doi:10.1016/j.devcel.2014.05.022.
53. Frick, C.L.; Yarka, C.; Nunns, H.; Goentoro, L. Sensing relative signal in the Tgf- $\beta$ /Smad pathway. *Proceedings of the National Academy of Sciences* **2017**, *114*, Not available. doi:10.1073/pnas.1611428114.
54. Kretzschmar, M.; Doody, J.; Timokhina, I.; Massague, J. A mechanism of repression of TGF $\beta$  / Smad signaling by oncogenic Ras. *Genes & Development* **1999**, *13*, 804–816. doi:10.1101/gad.13.7.804.
55. Míguez, D.G.; Gil-Guiñón, E.; Pons, S.; Martí, E. Smad2 and Smad3 cooperate and antagonize simultaneously in vertebrate neurogenesis. *Journal of Cell Science* **2013**, Not available, Not available. doi:10.1242/jcs.130435.
56. Sanz, A.L.; Míguez, D.G. Dual R-Smads interplay in the regulation of vertebrate neurogenesis. *Neurogenesis* **2014**, *1*, e29529. doi:10.4161/neur.29529.
57. Schmierer, B.; Tournier, A.L.; Bates, P.A.; Hill, C.S. Mathematical modeling identifies Smad nucleocytoplasmic shuttling as a dynamic signal-interpreting system. *Proceedings of the National Academy of Sciences* **2008**, *105*, 6608–6613. doi:10.1073/pnas.0710134105.
58. Khatibi, S.; Zhu, H.J.; Wagner, J.; Tan, J.; Burgess, A.W. Mathematical model of TGF-  $\beta$  signalling: feedback coupling is consistent with signal switching. *BMC Systems Biology* **2017**, *11*, 48. doi:10.1186/s12918-017-0421-5.
59. Chen, W.W.; Niepel, M.; Sorger, P.K. Classic and contemporary approaches to modeling biochemical reactions. *Genes & Development* **2010**, *24*, 1861–1875. doi:10.1101/gad.1945410.
60. Hangos, K.M.; Szederkényi, G. Mass action realizations of reaction kinetic system models on various time scales. *Journal of Physics: Conference Series* **2011**, *268*, 012009. doi:10.1088/1742-6596/268/1/012009.
61. CM Guldberg, P Waage, Ueber die chemische Affinität. 1. Einleitung (1879).
62. Berthollet, C.L. *Essai de statique chimique*; A Paris : Chez Firmin Didot ..., 1803.
63. Van'T Hoff, J.H. Die Grenzebene, ein Beitrag zur Kenntniss der Esterbildung. *Berichte der deutschen chemischen Gesellschaft* **1877**, *10*, 669–678. doi:10.1002/cber.187701001185.
64. Weiss, L. A simple demonstration of the law of conservation of mass. *Journal of Chemical Education* **1943**, *20*, 579. doi:10.1021/ed020p579.
65. Schummer, J., The Philosophy of Chemistry. In *Philosophy Of Chemistry: Synthesis of a New Discipline*; Baird., Ed.; Springer Netherlands: Dordrecht, 2006; pp. 19–39. doi:10.1007/1-4020-3261-7\_2.

**Disclaimer/Publisher's Note:** The statements, opinions and data contained in all publications are solely those of the individual author(s) and contributor(s) and not of MDPI and/or the editor(s). MDPI and/or the editor(s) disclaim responsibility for any injury to people or property resulting from any ideas, methods, instructions or products referred to in the content.